Arbitrary multi-way parallel mathematical operations based on planar discrete metamaterials

Yongle Wu[1, a)], Zheng Zhuang[1, b)], Li Deng[2, c)], Yuanan Liu[1], Quan Xue[3] & Zabih Ghassemlooy[4]

[1]Beijing Key Laboratory of Work Safety Intelligent Monitoring, School of Electronic Engineering, Beijing University of Posts and Telecommunications, P.O. Box. 282, 100876, Beijing, China.

[2]Beijing Key Laboratory of Network System Architecture and Convergence, School of Information and Communication Engineering, Beijing University of Posts and Telecommunications, P.O. Box. 282, 100876, Beijing, China.

[3]The State Key Laboratory of Millimeter Waves, Department of Electronic Engineering, CityU Shenzhen Research Institute, City University of Hong Kong, Hong Kong.

[4]Optical Communications Research Group, NCRLab, Faculty of Engineering and Environment, Northumbria University, Newcastle upon Tyne, NE1 8ST, U.K.

Contents

Abstract: Multi-way parallel mathematical operations along arbitrary transmission paths are constructed based on realizable planar discrete metamaterials in this paper. The introduced method of "computational metamaterials" is used to perform the desired mathematical operations. For producing high-efficiency devices, the function of multi-way parallel mathematical operations is indispensable in advanced analog computers. Therefore, in this paper we propose the arbitrary transmission paths that can be implemented by the bending of the electromagnetic waves based on the finite embedded coordinate transformations, which has a strong potential to realize the function of multi-way parallel computation. Nevertheless, owing to the inherent inhomogeneous property, metamaterials are difficult to be achieved in nature currently. In order to make it possible for fabricating in practical applications, the planar discrete metamaterial is a promising medium due to its homogeneous property. Numerical simulations validate the novel and effective design method for parallel optical computation.

Key words: multi-way, discrete metamaterials, mathematical operations, arbitrary transmission paths.

---

[a]Yongle Wu, [b]Zheng Zhuang, and [c]Li Deng contributed equally to this work.

[a]ywu@bupt.edu.cn.

I. Introduction

Traditional mathematical operations generally were performed in the past by analog computers in the form of mechanical [1] and electronic computers [2], which has been applied in various industrial applications including telecommunications, biomedicine, artificial intelligence, etc. However, these conventional analog computers have suffered from burning problems such as the slow response and a large size. Fortunately, in the rapidly changing technology age, optical computation brings about a brand-new concept to execute mathematical operations with an ultra-fast response in a relatively small size space.

In recent years, we have seen a growing research interest in optical computation, which promises to deliver processing performance exponentially faster and more powerful than the existing computing technologies [3-9]. Fast and stable optical computation based on the micro-waveguides with loss using the operator marching method (OMM) has been reported to solve the Helmholtz equation efficiently with complex refractive index or wavenumber [5]. This is followed by the development of optical computation of the spatial Laplace operator on the electromagnetic field components of the incident beam using the phased-shifted Bragg grating (PSBG) [6]. In order to accurately compute optical wave propagation in the inhomogeneous waveguides, a modified operator marching method based on a new treatment for local base transformation was proposed [7]. In addition, a novel concept of "computational metamaterials" based on dedicated metamaterial blocks is introduced, which can perform mathematical operations including spatial differentiation, integration, or convolution on the profile of electromagnetic waves as it propagates through the blocks [8]. Furthermore, another new concept of "metalines" for manipulating graphene plasmon (GP) waves is employed to realize analog computations on an ultra-compact planar graphene-based configuration [9]. Although all aforementioned schemes can efficiently achieve analog computations, the underlining mathematical theories generally have a major limitation associated with the complex fabrication in practical applications due to their inhomogeneous property.

In this paper, we present a novel scheme of performing the desired mathematical operations based on the easy-realizable planar medium, which is implemented on the basis of inhomogeneous metamaterials with the proper

design of permittivity according to the discrete theory [10]. Therefore, the proposed scheme is composed of a number of discrete units with basic homogeneous material parameters, which can be easily synthesized by the graphene when injected with the suitable external gate voltage [9], the tensor transmission lines [11], or 3D dielectric polyjet printing technology [12], etc. It is clear from the forgoing discussion that the designed discrete metamaterials would be a crucial step from the concept to reality in optical computation. We demonstrate the influence of discretization on mathematical operations through rigorous error analysis of the discrete degree. Furthermore, in order to achieve high efficient mathematical operations, the multi-way parallel operations have to be considered. By using finite embedded coordinate transformations, the transmission paths of incident waves can be bended arbitrarily on an anisotropic medium. Therefore, the essential function of arbitrary multi-way parallel mathematical operations for the advanced analog computers is achieved by means of controlling the transmission paths of incident waves based on the theory of transformation optics [13-15]. It should be noted that transformation optics is unlimited for the geometrical planar configuration, thus resulting in the possible of higher-efficiency multi-way operations. For convenience, the planar configuration is used to design and simulate multi-way parallel mathematical operations in this paper. Additionally, different from previous research works on transformation optics, the proposed scheme adopted easy-realizable planar discrete metamaterials as the designed medium. Hence, the proposed novel method of mathematical operations based on the planar discrete metamaterials offers certain advantages over the existing methods including that: *i*) two-dimensional or three-dimensional multi-way parallel operation with higher efficiency, *ii*) arbitrary controllable transmission paths, and *iii*) easy-realizable planar medium comprised of discrete metamaterials.

II. Multi-way parallel mathematical operations with metamaterials

As shown in Figure 1, the proposed system is composed of four cascaded sub-modules of *i*) a transformation optics for controlling the transmission paths of incident waves (anisotropic medium), *ii*) a Fourier transform (GRIN (+)), *iii*) a metasurface (MS) filter for obtaining the desired output function in the Fourier domain (MS), and iv) an inverse

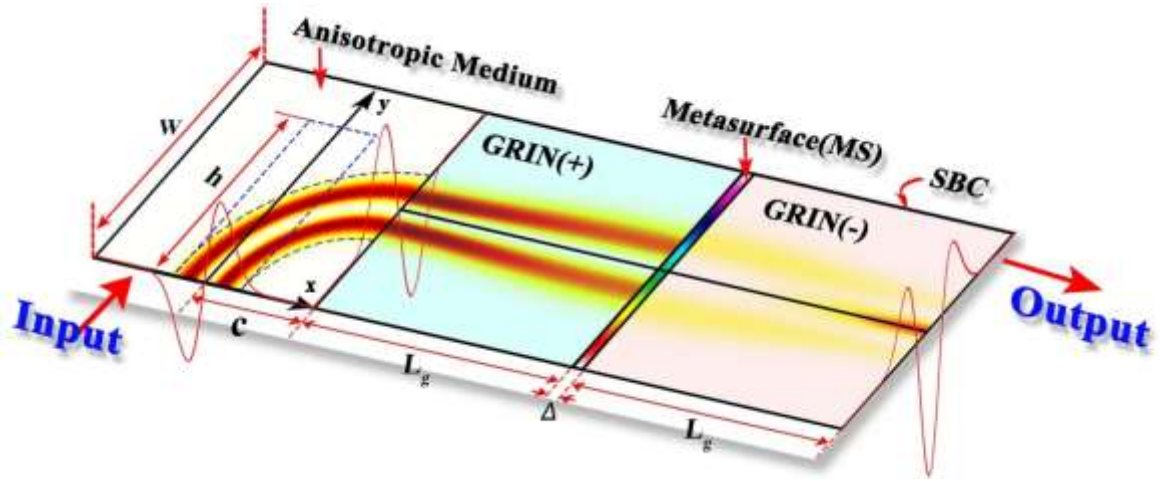

Figure 1 |. Ideal model of metamaterials-based computing system. The whole designed system is limited by the width W in the transverse direction y and by the total length $2(c+L_g)+\Delta$ in the longitudinal direction x. Consider an appropriate coordinate transformation in the anisotropic medium, the 90°-wave bending with radius c is realized to control the transmission paths of the incident wave. The two GRIN blocks (GRIN (+) and GRIN (-)) with positive and negative parameters are utilized to perform the Fourier transform and the inverse Fourier transform, respectively. And then the desired mathematical operations can be worked out in the metasurface (MS) with pre-defined permittivity and permeability.

Fourier transform (GRIN (-)).

For the 1st sub-modules, the permittivity ε_{ij}' and permeability μ_{ij}' of the transformation optical medium can be determined using the following expressions [14]:

$$\varepsilon_{ij}^{'} = \frac{AA^T}{\det(A)}\varepsilon_{ij}, \quad \mu_{ij}^{'} = \frac{AA^T}{\det(A)}\mu_{ij}, \tag{1}$$

where ε_{ij} and μ_{ij} are the constitutive parameter in the original space, respectively, and A^T indicates the transposed matrix of the Jacobi matrix of the transformation A, which is given as:

$$A = \frac{\partial(x', y', z')}{\partial(x, y, z)}. \tag{2}$$

Therefore, an appropriate coordinate transformation centered at the origin for wave-bending in the anisotropic medium can be prescribed by [15]:

$$\begin{cases} x' = x\cos\left(\dfrac{\theta y}{h}\right) \\ y' = x\sin\left(\dfrac{\theta y}{h}\right), \\ z' = z \end{cases} \tag{3}$$

where θ is the radian of the bending angle and h denotes the length of the original incident wave. If the original space is free space, then the values of ε_{ij} and μ_{ij} are ε_0 and μ_0, respectively. According to equations (1)-(3), the relative permittivity and permeability in the transformed medium can be obtained by [15]:

$$\varepsilon_r^{'} = \frac{\varepsilon_{ij}^{'}}{\varepsilon_0} = \begin{pmatrix} \frac{1}{kr}\left(\frac{(x-x_0)^2}{r^2} + k^2(y-y_0)^2\right) & \frac{(x-x_0)(y-y_0)}{kr}\left(\frac{1}{r^2} - k^2\right) & 0 \\ \frac{(x-x_0)(y-y_0)}{kr}\left(\frac{1}{r^2} - k^2\right) & \frac{1}{kr}\left(\frac{(y-y_0)^2}{r^2} + k^2(x-x_0)^2\right) & 0 \\ 0 & 0 & \frac{1}{kr} \end{pmatrix} = \frac{\mu_{ij}^{'}}{\mu_0} = \mu_r^{'}, \tag{4}$$

where $r = \sqrt{(x-x_0)^2 + (y-y_0)^2}$ and $k = \theta/h$. It should be noted that x_0 and y_0 are the center coordinate of wave-bending. For simplicity, the values of θ and h are set as $\pi/2$ and λ_0 in this work, respectively. Hence, the transmission direction of an incident wave can be controlled by x_0 and y_0 artificially so that different coordinate transformations can make it possible for arbitrary multi-way parallel operation.

As for the other three sub-modules, we have adopted the concept of "computational metamaterials" developed by *silva et al*. **[Science 343, 160 (2014)]** to perform the desired mathematical operations. For the purpose of making GRIN (+) slab operate as a Fourier transformer, the material parameters of GRIN (+) are defined as [8]:

$$\varepsilon(y) = \varepsilon_c\left[1 - \left(\frac{\pi}{2L_g}\right)^2 (y \pm c)^2\right], \text{ and } \mu(\text{y}) = \mu_0, \tag{5}$$

where ε_c is the permittivity at the central plane of the GRIN and L_g is the characteristic length. Similarly, for the inverse Fourier transform, the material parameters of GRIN (-) should be negative. Considering n-order differentiation, the relative permittivity and permeability of the inhomogeneous MS with thickness Δ can to be deduced as [8]:

$$\frac{\varepsilon_{ms}(y)}{\varepsilon_0} = \frac{\mu_{ms}(y)}{\mu_0} = in\left(\frac{\lambda_0}{2\pi\Delta}\right)\ln\left(\frac{-iW}{2(y \pm c)}\right), \text{ for } |y| \le W/2, \tag{6}$$

where '±' denotes the center position of the GRIN along the y-axis.

To sum up, combining transformation optics with the concept of computational metamaterials, arbitrary multi-way parallel mathematical operation can be implemented with the planar inhomogeneous medium. To confirm the validity of

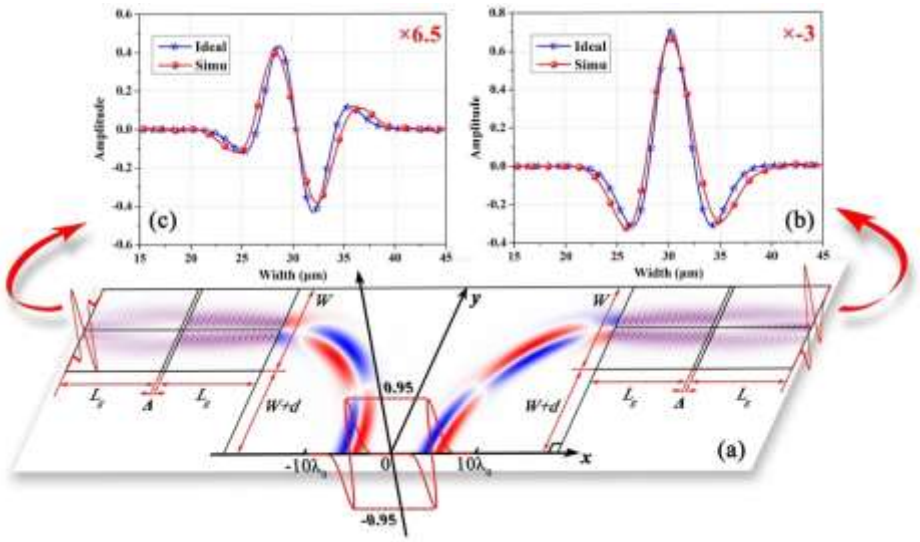

Figure 2 |. Two-to-two-way parallel mathematical operations with metamaterials (TTWPMOM); (a) snapshots of the electric field distribution for the z-component with designed first- and second-order differentiators; (b) and (c) simulation results of parallel mathematical operations at the output terminal for (b) first-order differentiation and (c) second-order differentiation. The dimensions are W=10λ_0=30 μm, L_g=11.67λ_0=35 μm, Δ=1 μm, d=λ_0/8=0.375 μm, and λ_0=3 μm. Note that the range of horizontal axis in (b) and (c) are depended on the designed vertical position of differentiator. For facilitating the comparison, output results are multiplied by the constant factor indicated in the top corner of the panel.

this method, we carry out full wave simulations using the multiphysics simulation tool as a finite element solver. Furthermore, to estimate the errors due to discretization and numerical simulations, the mean squared error (*MSE*) and the coefficient of determination (R^2) in signal processing are used, which are given as [16]:

$$MSE = \frac{1}{n}\sum_{i=1}^{n}[I_i - S_i]^2, \tag{7}$$

and

$$\begin{cases} R^2 = 1 - \dfrac{RSS}{TSS} \\ RSS = \displaystyle\sum_{i=1}^{n}[I_i - S_i]^2, \\ TSS = \displaystyle\sum_{i=1}^{n}[I_i - \overline{I}_i]^2 \end{cases} \tag{8}$$

where I_i and S_i are the numerical values of ideal and simulated curves, respectively. As expected with $MSE \rightarrow 0$ and $R^2 \rightarrow 1$, the errors will be smaller. The corresponding simulation cases of the multi-way parallel mathematical operations with multi-input are illustrated in Figures 2 and 3, respectively. First, the input function $f(x) = a(x-c')e^{-(x-c')^2/b}$, with a=0.7 μm and b=10 μm, is performed at the bottom of the designed panel while the output results are displayed on two sides of the panel. Note that the value of c' is depended on the position of zero point of the input function. Next, for the

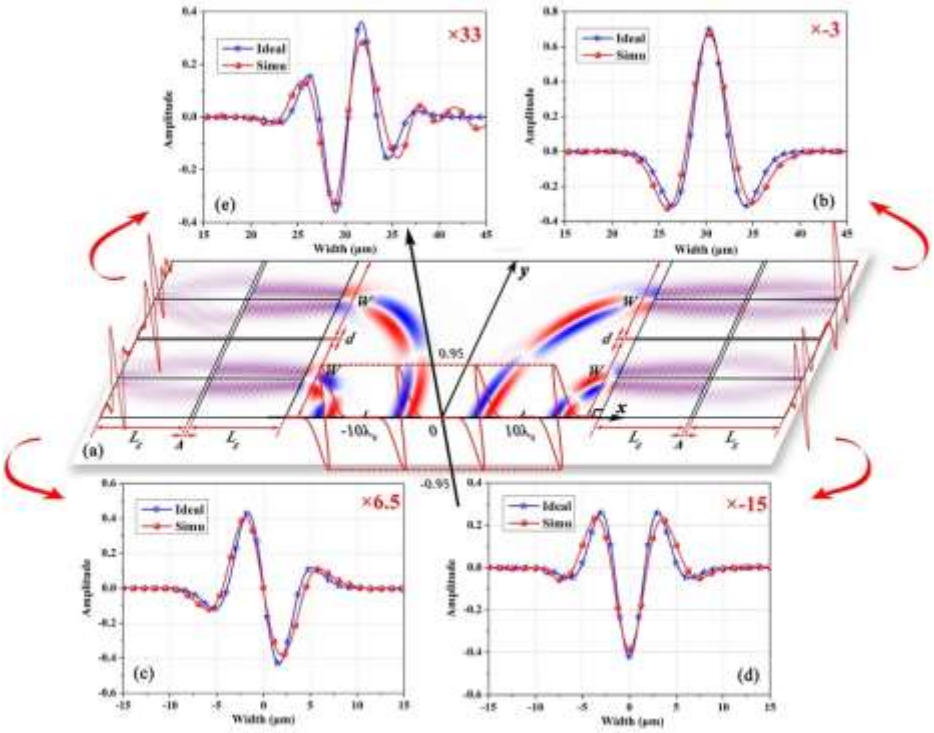

Figure 3 |. Four-to-four-way parallel mathematical operations with metamaterials (FFWPMOM); (a) snapshots of the electric field distribution for the z-component with the designed first-order to forth-order differentiator; (b) to (e) simulation results of parallel mathematical operations at the output terminal for (b) first-order differentiation, (c) second-order differentiation, (d) third-order differentiation, and (e) forth-order differentiation. The dimensions are $W=10\lambda_0=30$ μm, $L_g=11.67\lambda_0=35$ μm, $\Delta=1$ μm, $d=\lambda_0/8=0.375$ μm, and $\lambda_0=3$ μm. Note that the ranges of horizontal axis in (b)-(e) are depended on designed vertical position of differentiator. For facilitating the comparison, output results are multiplied by the constant factor indicated in the top corner of the panel.

TABLE I. All the designed parameters for multi-way parallel mathematical operations with *n*-order differential.

	W (μm)	L_g (μm)	Δ (μm)	d (μm)	x_0 (μm)	y_0 (μm)	h (μm)	θ (rad)
TTWPMOM	30	35	1	0.375	±60.375	-15	3	π/2
FFWPMOM	30	35	1	0.375	±60.375	-15	3	π/2
OTWPMOM	30	35	1	-	30	-15	3	π/2
TTWPMODM	30	35	1	0.545	±60.545	-15	3	π/2

sub-modules of transformation optics, the medium parameters are determined using (4). Due to the symmetry, the parameters of the right and left sides in transformation optical sub-modules are identical except for the "±" of center coordinate of wave-bending (i.e., x_0, y_0). Moreover, the design parameters of transformation optical sub-modules in Figure 2 are also identical to those used in Figure 3 due to the same input position and center coordinate of wave-bending. In other words, the proposed method theoretically can provide arbitrary multi-way transmissions with the same design parameters. Finally, the medium parameters in mathematical operations are calculated using (5) and

TABLE II. The calculated values of MSE and R2 for designed multi-way parallel mathematical operations with n-order differential.

	1st differential		2nd differential		3rd differential		4th differential	
	MSE	**R^2**	**MSE**	**R^2**	**MSE**	**R^2**	**MSE**	**R^2**
TTWPMOM	0.0030	0.9380	0.0021	0.9123	-	-	-	-
FFWPMOM	0.0028	0.9409	0.0018	0.9262	0.0014	0.9161	0.0020	0.8677
OTWPMOM	0.0032	0.9327	0.0020	0.9164	-	-	-	-
TWPMODM	0.0031	0.9348	0.0029	0.8780	-	-	-	-

(6). In addition to the dimensions indicated in Figures 2 and 3, the design parameters in all aforementioned equations are assumed as $x_0=\pm(2W+d)= \pm 60.375$ μm, $y_0=W/2=15$ μm, $k=\theta/h=\pi/6$ rad▪μm^{-1}, and $\varepsilon_c=2.01\varepsilon_0$. For convenience, all the designed parameters are illustrated in Table I. As shown in Figures 2 and 3, the arbitrary transmission paths can be implemented based on 90°-wave bending using equations (1)-(4), whereas the mathematical operations are performed based on equations (5) and (6). As a comparison, the ideal plots are depicted in Figures 2(b)-(c) and Figures 3(b)-(e) based on derivate of the input function $f(x)=a(x-c')e^{-(x-c')^2/b}$. It is clear that there are excellent agreements between simulated and the ideal plots, thus confirming the function of parallel mathematical operations. In order to further assess and prove the reliability of the proposed method, the values of *MSE* and R^2 are calculated according to (7) and (8) as illustrated in Table II. For the two-way parallel mathematical operations with two-input, the values of *MSE* for 1st- and 2nd-derivate are 0.0030 and 0.0021, respectively, and the values of R^2 for 1st- and 2nd-derivate are 0.9380 and 0.9123. For the four-way parallel mathematical operations with four-input, the values of *MSE* for 1st-, 2nd-, 3rd, and 4th-derivate are 0.0028, 0.0018, 0.0014 and 0.0020, respectively, and the values of R^2 for 1st-, 2nd-, 3rd, and 4th-derivate are 0.9409, 0.9262, 0.9161 and 0.8677, which further validate the proposed theory and method.

Besides the multi-way parallel mathematical operations with multi-input, the two-way parallel mathematical operation with only one input has also been investigated. The input function $f(x)=a(x-c')e^{-(x-c')^2/b}$, with a=0.7 μm and b=10 μm, is performed at the center of the designed transformation optical sub-modules with medium parameters calculated using (4). All the key designed parameters are illustrated in Table I. There is a good agreement between simulated and the ideal plots as shown in Figures 4(b) and 4(c). In order to further validate the proposed theory and

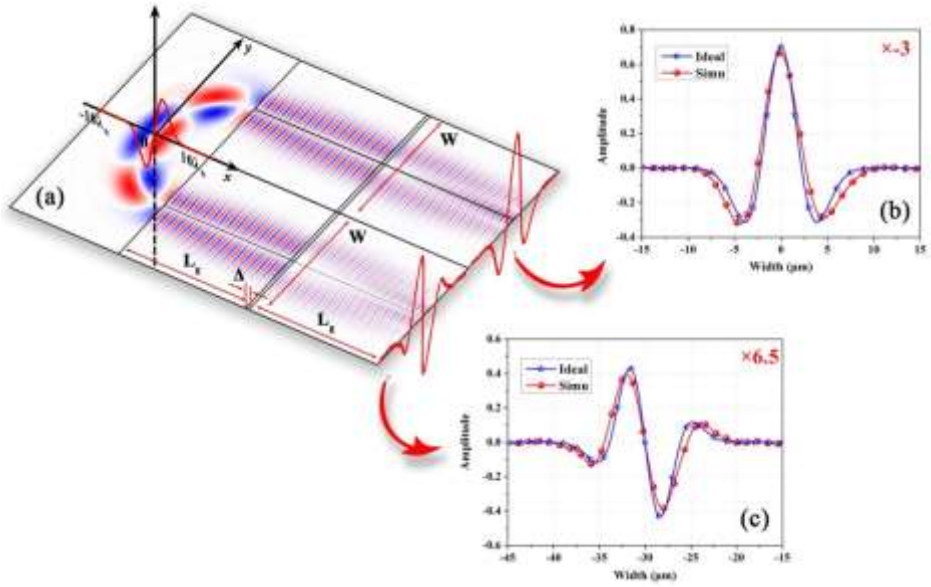

Figure 4 |. One-to-two-way parallel mathematical operations with metamaterials (OTWPMOM); (a) snapshots of the electric field distribution for the z-component with designed first- and second-order differentiators; (b) and (c) simulation results of parallel mathematical operations at the output terminal for (b) first-order differentiation and (c) second-order differentiation. The dimensions are $W=10\lambda_0=30$ μm, $L_g=11.67\lambda_0=35$ μm, $\Delta=1$ μm, and $\lambda_0=3$ μm. Note that the range of horizontal axis in (b) and (c) are depended on the designed vertical position of differentiator. For facilitating the comparison, output results are multiplied by the constant factor indicated in the top corner of the panel.

method, the values of *MSE* and R^2 are calculated based on (7) and (8) as illustrated in Table II.

III. Multi-way parallel mathematical operations with discrete metamaterials

Although parallel mathematical operations are realized by introducing the concept of "computational metamaterials", it is rather challenging to realize practically due to its inhomogeneous property. Therefore, for fabrication purposes the method of discrete metamaterials is adopted as outlined in this section. As illustrated in Figures 5 and 6(a), original four cascaded sub-modules are decomposed into a number of discrete units with the dimension *g*. The homogeneous materials parameters of transformation optical sub-modules are needed to be rewritten as:

$$\varepsilon_r^{"}=\mu_r^{"}=\begin{pmatrix} \frac{1}{kr}\left(\frac{(g_0+ng-x_0)^2}{r^2}+k^2(g_0+ng-y_0)^2\right) & \frac{(g_0+ng-x_0)(g_0+ng-y_0)}{kr}\left(\frac{1}{r^2}-k^2\right) & 0 \\ \frac{(g_0+ng-x_0)(g_0+ng-y_0)}{kr}\left(\frac{1}{r^2}-k^2\right) & \frac{1}{kr}\left(\frac{(g_0+ng-y_0)^2}{r^2}+k^2(g_0+ng-x_0)^2\right) & 0 \\ 0 & 0 & \frac{1}{kr} \end{pmatrix},\quad n=0,1,2,..., \tag{9}$$

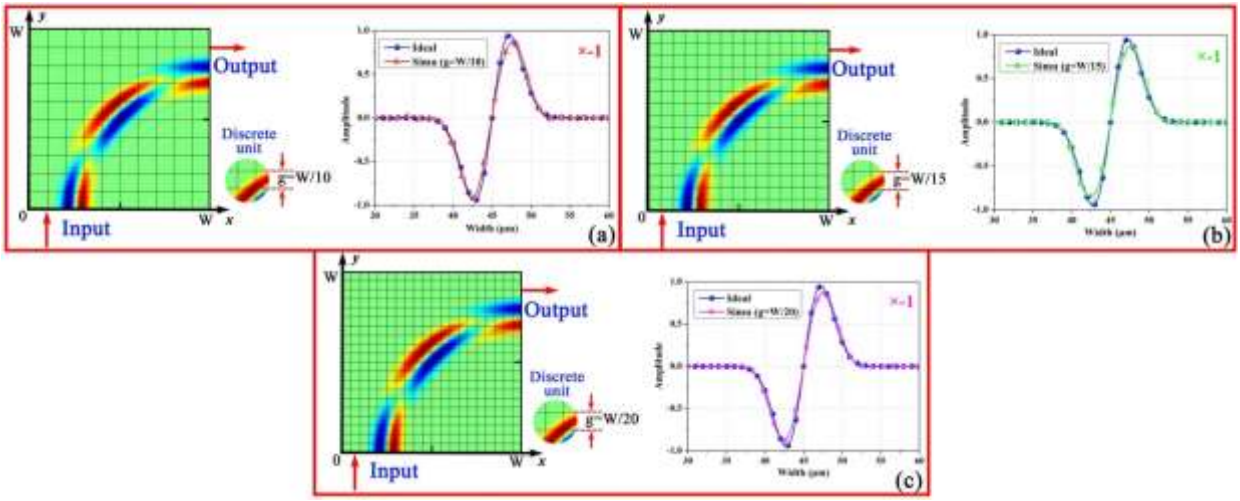

Figure 5 |. Simulation results for discretization of 90°-wave bending; (a) the size of discrete unit is 6×6 μm^2 (W=60 μm), and the calculated values of *MSE* and R^2 are 0.0026 and 0.9837; (b) the size of discrete unit is 4×4 μm^2, and the calculated values of *MSE* and R^2 are 0.0025 and 0.9844; (c) the size of discrete unit is 3×3 μm^2, and the calculated values of *MSE* and R^2 are 0.0021 and 0.9869. Note that the range of horizontal axis in (a)-(c) is depended on the designed vertical position of output terminal.

where $r=\sqrt{(g_0+ng-x_0)^2+(g_0+ng-y_0)^2}$ and $g_0=g/2$. Similarly, the sub-modules of mathematical operations can be determined as follows:

$$\varepsilon^{'}=\varepsilon_c\left[1-\left(\frac{\pi}{2L_g}\right)^2(g_0+ng\pm c)^2\right],\ \mu^{'}=\mu_0, \tag{10}$$

and

$$\frac{\varepsilon_{ms}^{'}}{\varepsilon_0}=\frac{\mu_{ms}^{'}}{\mu_0}=in\left(\frac{\lambda_0}{2\pi\Delta}\right)\ln\left(\frac{-iW}{2(g_0+ng\pm c)}\right). \tag{11}$$

From equations (9)-(11), each of the discrete unit has basic homogeneous material parameters. Therefore, the discrete metamaterials will have a wider range of applications compared to the existing concepts. For the sake of depicting the impacts of discretization on the whole system, we have carried out simulations for discretization of 90°-wave bending and mathematical operations with different discrete degrees, respectively. As we can see in Figure 5, the simulated output plots are almost the same as the ideal input plots by 90°-wave bending even though the dimensions of discrete units are a bit large. Moreover, compared with the calculated corresponding *MSE* and R^2 for different discrete units' dimensions, the influence of discretization on the input distribution would decrease with the decreasing of the discrete units' dimensions. Besides, the simulated plots of the 1st differential in the discrete metamaterials shown

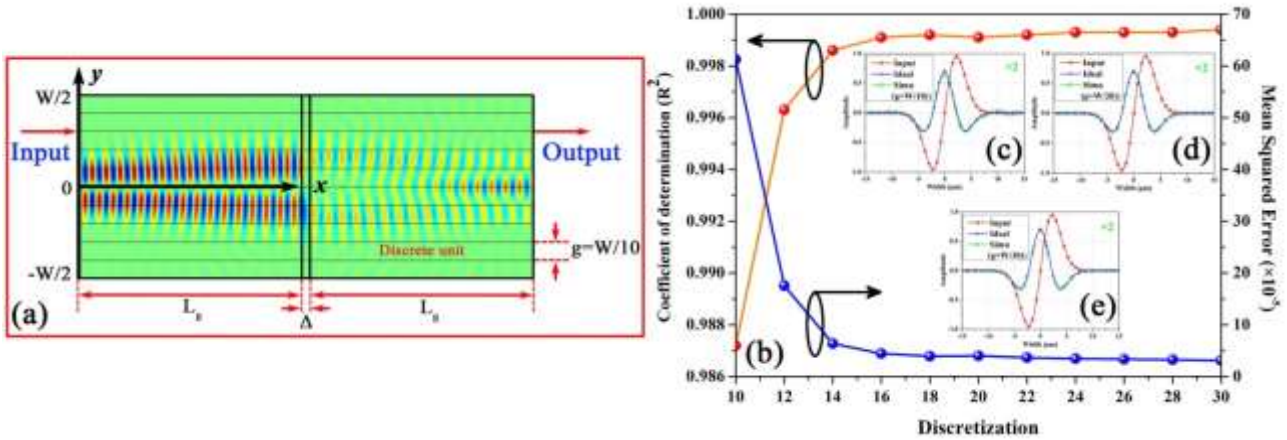

Figure 6 |. Simulation results for discretization of mathematical operations; (a) snapshots of the electric field distribution for the z-component of the designed first-order differentiator, with the size of discrete unit as 3×3 μm^2 (W=30 μm); (b) the curves of *MSE* and R^2 for different discrete units' dimensions. The ranges of discrete units' dimensions is from 3 μm (W/10) to 1 μm (W/30); (c)-(e) simulation results of mathematical operations at the output terminal for first-order differentiation with (c) g= W/10, (d) g= W/20, and (e) g=W/30.

in Figure 6 are nearly identical with the ideal plots from Figures 6(c)-(e). For further studying the possible errors of discrete metamaterials, the curves of *MSE* and R^2 for different discrete units' dimensions are depicted in Figure 6(b), which shows that the errors are decreased with the decreasing of the discrete units' dimensions according to the calculated *MSE* and R^2. Furthermore, even though the dimensions of discrete units are a bit large, the simulation results obtained still are excellent. Hence, the simulation involving two-way parallel mathematical operations with discrete metamaterials is implemented as shown in Figure 7. Note that all the designed parameters of the simulation in Figure 7 are almost identical with the simulation in Figure 2 except the value of d from Table I. As depicted on the bottom of the designed panel in Figure 7, the input function used is also the same as multi-way parallel mathematical operations with metamaterials, whereas the output results are displayed on two sides of the panel. The calculated values of *MSE* and R^2 are outlined in Table II. As we can see, the values of *MSE* are almost 0.003 and the values of R^2 are greater than 90% for most, thus confirming the feasibility and viability of the proposed novel method.

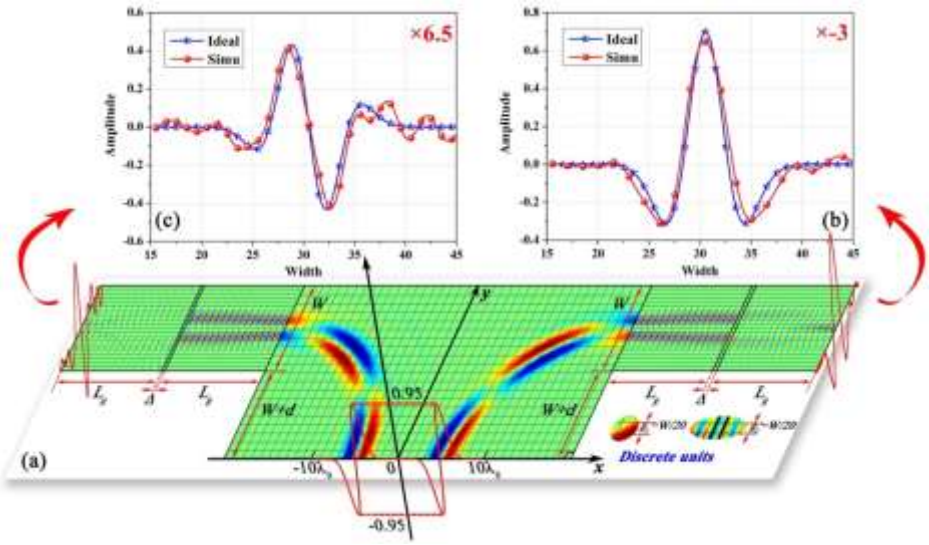

Figure 7 |. Two-to-two-way parallel mathematical operations with discrete metamaterials (TWPMODM); (a) snapshots of the electric field distribution for the z-component with the designed first- and second-order differentiators; (b) and (c) simulation results of parallel mathematical operations at the output terminal for (b) first-order differentiation and (c) second-order differentiation. The dimensions are $W=10\lambda_0=30$ μm, $L_g=11.67\lambda_0=35$ μm, $\Delta=1$ μm, $d=\lambda_0/5.5=0.545$ μm, and $\lambda_0=3$ μm. Note that the ranges of horizontal axis in (b) and (c) are depended on the designed vertical position of differentiator. For facilitating the comparison, output results are multiplied by the constant factor indicated in the top corner of the panel.

IV. Discussion

Multi-way parallel mathematical operations are performed based on the discrete metamaterials in this paper. Apart from the excellent function of mathematical operations, the proposed structure can effectively achieve arbitrary multi-way transmission paths. To make it straight forward and relative easy for fabrication, we introduced the concept of discrete metamaterials for realizing the homogeneous property. Although the simulation results depicted in Table II indicate that the discrete metamaterials will result in errors comparing with MS, the errors almost do not affect the expected mathematical operations. Moreover, the errors can be reduced by increasing the dimension of discrete unit based on Figure 6(b). Although no experimental validation of the proposed method has been outlined in this paper, we have validated the theory by means of excellent simulation results and the corresponding calculated MSE/R^2.

In recent years, for experimental validation of metamaterials, researches have provided a number of effective methods, including the graphene with the suitable external gate voltage [9], the tensor transmission lines [11], or 3D dielectric polyjet printing technology [12], etc. In [9], by applying appropriate external gate voltage and a well-designed

ground plane thickness profile beneath the dielectric spacer holding the graphene layer, the desired homogeneous surface conductivity values used to calculate metamaterial parameters can be obtained at different segments of the graphene layer. Additionally, based on the designed tensor transmission-line metamaterial unit cell in [11], an isotropic and homogeneous medium was achieved with the calculated permeability tensor and permittivity. Recently, an all-dielectric lens prototype based on transformation optics was fabricated using 3D dielectric polyjet printing technology [12]. However, the most basic condition for achieving these schemes is the homogeneous material parameter. Therefore, the proposed novel method in this paper not only produces high-efficient parallel mathematical operations, but also is the essential step from the concept to the reality in optical computation, which makes it possible for further experimental validation.

V. Methods

The simulated results are obtained by using the multiphysics simulation tool based on the finite element method (FEM). In all simulations, the whole system is contained within a cascaded area with scattering boundary condition (SBC). The corresponding values of *MSE* and R^2 are calculated according to equations (7)-(8).

Acknowledgement

This work was supported in part by National Natural Science Foundations of China (No.61422103, and No.61671084), and National Key Basic Research Program of China (973 Program) (No.2014CB339900).

References

1. Solla P. D. A history of calculating machines. *IEEE Micro* **4**, 22-52 (1984).
2. Clymer A. B. The mechanical analog computers of Hannibal Ford and William Newell. *IEEE Annals of the History of Computing* **2**, 19-34 (1993).
3. Engheta N. 150 years of Maxwell's equations. *Science* **349**, 136-137(2015).

4. Sihvola A. Enabling optical analog computing with metamaterials. *Science* **343**, 144-145 (2014).
5. Zhu J. & Song R. Fast and stable computation of optical propagation in micro-waveguides with loss. *Microelectronics Reliability* **49**, 1529-1536 (2009).
6. Bykov D. A., Doskolovich L. L., Bezus E. A. & Soifer V. A. Optical computation of the Laplace operator using phase-shifted Bragg grating. *Optics Express* **22**, 25084-25092 (2014).
7. Zhu J. & Wang G. High-precision computation of optical propagation in inhomogeneous waveguides. *JOSA A* **32**, 1653-1660 (2015).
8. Silva A., Monticone F., Castaldi G., Galdi V., Alù A. & Engheta N. Performing mathematical operations with metamaterials. *Science* **343**, 160-163 (2014).
9. AbdollahRamezani S., Arik K., Khavasi A. & Kavehvash Z. Analog computing using graphene-based metalines. *Optics Letters* **40**, 5239-5242 (2015).
10. Huang Y., Feng Y. & Jiang T. Electromagnetic cloaking by layered structure of homogeneous isotropic materials. *Optics Express* **15**, 11133-11141(2007).
11. Gok G. & Grbic A. Tensor transmission-line metamaterials. *IEEE Trans. Antennas and Propagation* **58**, 1559-1566 (2010).
12. Yi J., Burokur S. N., Piau G. P. & Lustrac A. D. Coherent beam control with an all dielectric transformation optics based lens. *Scientific Reports* **6**, (2016).
13. Rahm, M., Roberts, D. A., Pendry, J. B. & Smith, D. R. Transformation-optical design of adaptive beam bends and beam expanders. *Optics Express* **16**, 11555-11567 (2008).
14. Pendry J. B., Schurig D. & Smith D. R. Controlling electromagnetic fields. *Science* **312**, 1780-1782 (2006).
15. Jiang W. X., Cui T. J., Zhou X. Y., Yang X. M. & Cheng Q. Arbitrary bending of electromagnetic waves using realizable inhomogeneous and anisotropic materials. *Physical Review E* **78**, 066607 (2008).
16. Dougherty E. R., Kim S. & Chen Y. Coefficient of determination in nonlinear signal processing. *Signal Processing* **80**, 2219-2235(2000).